frontiers | Frontiers in Earth Science

TYPE Original Research
PUBLISHED 13 September 2022
DOI 10.3389/feart.2022.1013715

OPEN ACCESS

EDITED BY
Hongtu Zhang,
Henan Polytechnic University, China

REVIEWED BY
Lianpeng Dai,
Liaoning University, China
Bo Zhao,
Taiyuan University of Technology, China
Gan Feng,
Sichuan University, China

*CORRESPONDENCE
Sheng Li,
13941811946@139.com

SPECIALTY SECTION
This article was submitted to Economic Geology,
a section of the journal
Frontiers in Earth Science

RECEIVED 07 August 2022
ACCEPTED 25 August 2022
PUBLISHED 13 September 2022

CITATION
Jia C, Li S, Fan C, Luo M, Yang Z, Yang L and Pu Z (2022), Instability and failure characteristics of surrounding rock of water drenching roadway in thick coal seam.
Front. Earth Sci. 10:1013715.
doi: 10.3389/feart.2022.1013715

Instability and failure characteristics of surrounding rock of water drenching roadway in thick coal seam

Ce Jia[1], Sheng Li[1]*, Chaojun Fan[1], Mingkun Luo[2], Zhenhua Yang[1], Lei Yang[1] and Ziang Pu[1]

[1]College of Mining, Liaoning Technical University, Fuxin, China, [2]Institute of Science and Technology, Shanxi Lu'an Chemical (Group) Co., Ltd., Changzhi, China

Aiming at the water drenching problem in the roof of transport roadway 2,606 of the Zhangcun coal mine, the instability and failure law of the drenching roadway was studied by borehole peephole, soaking water softening test and numerical simulation in this study. It is found that the relation between compressive strength, elastic modulus, tensile strength and moisture content is a negative exponential function. Subsequently, the Fish language was used to embed the functional relationship between mechanical parameters of surrounding rock in the roadway and moisture content into Flac^{3D} software to simulate the failure law of surrounding rock under different moisture contents. The influence of moisture content on the surrounding rock is ordered as roof > two sides > floor. Through the comparison between borehole peeping and plastic zone, the roof water content is obtained by inversion. The results provide a reference basis for the selection of the surrounding rock support method for drenching roadway in thick coal seam.

KEYWORDS

water drenching roadway, water-rock coupling, surrounding rock deformation, particle flow, borehole peephole

Introduction

China has a wide distribution of coal resources, and is the largest coal producer in the world (Xie et al., 2018; Fan et al., 2020). Nearly 76.3% of coal resources are buried above 600 m, and 59.5% are buried above 1,000 m (Su et al., 2021; Wang et al., 2022). Due to the increase in mining intensity, the depth of coal mining in China is increasing with a growth rate of 8–12 m per year (Fan et al., 2022a). With the increase of mining depth, geological anomalies, roof permeability, and other problems have been encountered during the mining process (Yang et al., 2017a; Chen et al., 2021; Dou et al., 2021). To effectively control the roadway surrounding rock, deformation characteristics and the mechanism of the roadway surrounding rock under the influence of water drenching and the control of roadway stability under the condition of water drenching roof have been widely concerned at present

(Gao et al., 2021; Zhao et al., 2022). The roadway surrounding rock under drenching conditions shows prominent soft rock characteristics. Therefore, the large deformation of roadway surrounding rock is difficult to control, which seriously hinders coal mines' high-yield and high-efficiency production (Zhu et al., 2022a; Fan et al., 2022b).

Recently, Li and He (He, 2014; Li et al., 2016; Fan et al., 2021) proposed that the deformation of the surrounding rock is caused by various factors such as soft features, poor support, high ground stress, groundwater, and geological formations. The research on the surrounding rock control technology of water drenching and soft rock roadways is mainly carried out through numerical simulation, industrial tests, and laboratory tests (Zhang et al., 2016; Tao et al., 2020; Zhai et al., 2022). Yang (Yang et al., 2017b) revealed the damage mechanism of soft rock roadways under high stress, long-term water immersion conditions by numerical simulation and field industrial tests. Through scanning electron microscopy, Yu (Yu et al., 2021) obtained that the weakly cemented siltstone is composed of coarse-grained minerals with highly developed pores, revealing the instability of the soft rock roadway. Ma (Ma et al., 2021) conducted indoor experimental tests on red shale to obtain mineral composition and microstructure, anisotropy, hydraulic properties, and other mechanical parameters to reveal its deformation and damage characteristics. Besides, the damage law of the red shale soft rock roadway was obtained by the FLac^{3D} software. Wen (Wen et al., 2021) investigated the support method for large section soft rock roadway and obtained the displacement, plastic zone, and stress field distribution law of the surrounding rock by numerical simulation. By using the numerical simulation inversion, Chen (Chen et al., 2020) reported that as the moisture content increases, the failure zone further extends to the deep surrounding rock, leading to increased stress relaxation around the roadway, especially in the roof. Wei (Zhu et al., 2022b) proposed a new concept of internal and external self-bearing structures for the surrounding rock and determined the shape of the internal and external bearing structures based on the results of field monitoring. Through indoor tests, numerical calculations, and field tests, Li (Li et al., 2015) analyzed the composition and microstructure of mudstone and obtained the hydration law of mudstone and its characteristics of strength weakening as well as the deformation and damage characteristics of surrounding rock under the action of the hydration. Zheng (Zheng et al., 2021) studied the effects of different factors on the stability of soft rock roadways based on numerical simulation techniques. It was found that high ground stress, rock fragmentation, and poor lithology are the factors that lead to the instability of the roadway; besides, physical and mechanical properties of the surrounding rock and the bearing capacity of the surrounding rock layer can be promoted to maintain the stability of the roadway with broken soft rock. Chen (Chen et al., 2018) analyzed the mineral composition of the surrounding rock by X-ray diffraction. The results showed that the surrounding rock contains clay minerals that tend to expand upon water contact, leading to instability and damage of the surrounding rock of the roadway. Bai (Bai and Tu, 2016) analyzed the failure of large span long-wall roadways under water-rich roofs by field observation and numerical simulation, and found that large span excavation induces rock fracture to form seepage pathways. The water drenching not only weakens the rock mass but also reduces the bond between the surrounding rock and the anchor rods, resulting in the failure of the anchor rods and anchor cables.

In this study, the instability and damage law of the water drenching roadway was studied by drilling peephole, soaking water softening experiment, and numerical simulation to provide guidance for surrounding rock control of 2,606 transport roadway in Zhangcun coal Mine.

Research background

Zhangcun coal mine is located in Changzhi City, Shanxi Province. No.3 coal seam in the lower part of Shanxi Formation of Permian was exploited in working face 2,606. This coal seam has a stable occurrence, a small variation in coal thickness, and a simple coal seam structure. The buried depth of the coal seam is about 537 m, the thickness of the coal seam is 5.33–6.19 m, and the average thickness is 5.86 m. The original gas content during the tunneling of the transport roadway 2,606 was 8.5–10.0 m^3/t and the temperature was 15–17°C. Transport roadway 2,606 was located in the north of belt road 26, 300 m east from transport roadway 2,605. For transport roadway 2,606, the bottom of the coal seam was designed to be excavated, leaving 1.5–2 m thick top coal. The layout of the roadway and the design section of transport roadway 2,606 was 5.8m×4 m (length × width), as shown in Figure 1A. The direct top of No.3 coal seam roof was mudstone with a thickness of 2.49 m, and the old top above the direct top was medium and fine-grained sandstone, with a thickness of about 7.83 m. The direct bottom was mudstone, with a thickness of 2.83 m, and the old bottom was gray-white fine-grained sandstone, with a thickness of 5.04 m, as shown in Figure 1B.

According to the hydrogeological conditions of the mine, the No. VII water-bearing layer was 2.49 m below the No. 3 coal seam. The thickness of this water-bearing layer was 7.83 m, and its lithology was gray-white medium and fine-grained sandstone. During the excavation process, the roof water drenching occurred in transport roadway 2,606, and the water seeping down at the anchor pallet was collected through the drencher into the drainage tank. The roof water drenching led to the softening of the coal rock body, severe deformation of the roadway roof, and the corrosion of anchor rods and anchor cable pallets, as shown in Figure 2.

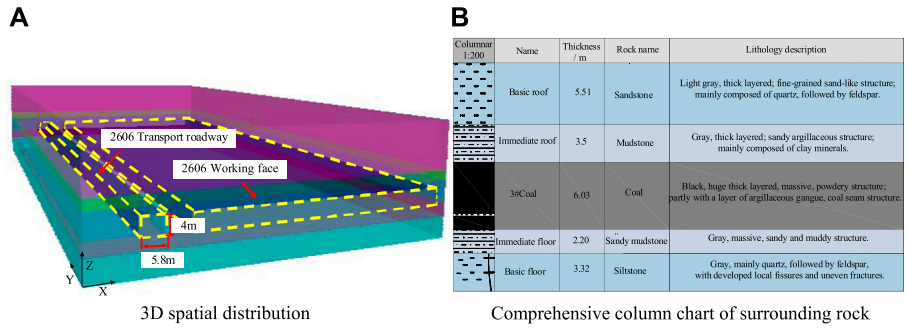

FIGURE 1
Geological overview of transport roadway 2,606. **(A)** 3D spatial distribution. **(B)** Comprehensive column chart of surrounding rock.

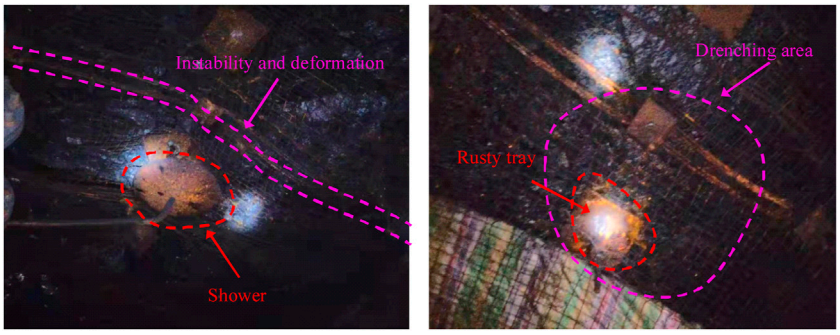

FIGURE 2
Roof drenching and damage pictures on-site.

Macroscopic evolution law of mudstone under the action of water-mechanical coupling

When mudstone encounters water, it will expand, argillite, disintegrate, and break, resulting in the softening of mudstone (Liu et al., 2020). The softening effect of water on rock is by affecting the microstructure of rock, resulting in the reduction of macroscopic mechanical properties. Therefore, the PFC^{2D} software was used to explore the mechanical properties and fracture evolution laws of mudstone under different water contents. PFC^{2D} software was used to build a cuboid sample with a model size of 100mm × 50 mm (length × width). The cuboid sample was composed of round particles. Due to the non-uniform characteristics of rock materials, the rock particle radius is randomly generated between 0.3 and 0.75 mm (Yang et al., 2019), and finally, the particles are continuously vibrated within the specified range to reach a balanced state. Uniaxial Compression and Tensile Testing of Rocks by Loading Walls, as shown in Figure 3.

Mudstone belongs to argillaceous cemented rock. To better reflect the mechanical properties of rock materials, the parallel cementation model (PBM) is used to simulate the rock laboratory test. According to the PFC micromechanical parameters analysis method introduced by U. Castro-Filgueira (Castro-Filgueira et al., 2017), a large number of trial calculations were carried out to determine the initial parameters of the model micromechanical parameters, as shown in Table 1. According to the literature (Zhao et al., 2021), it can be known that the water content influences the normal, tangential bond strength and bond strength ratio parameters of the rock. Combined with the data in the literature (He, 2021; Jing et al., 2021; Liu et al., 2021), the functions of rock normal, tangential bond strength, bond strength ratio, and water content are obtained.

$$\begin{cases} \sigma_c = 32\exp(-w/0.41) + 1.4 \\ \tau_c = 59\exp(-w/0.34) + 1.46 \\ k_c = -13.5\exp(-w/0.37) + 3.7 \end{cases} \quad (1)$$

Where: σ_c is the normal bond strength, MPa; τ_c is the tangential bond strength, MPa; k_c is the bond strength ratio; w is the moisture content, %.

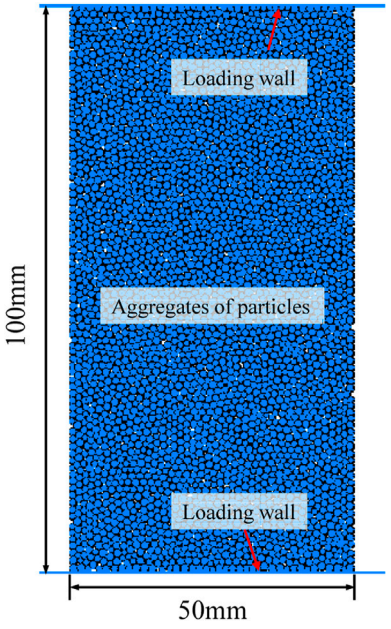

FIGURE 3
Generation of balls and walls.

Evolution law of mechanical properties of mudstone with different water content

Figure 4 shows the evolution law of mudstone mechanical properties under different water contents. In Figure 4A, the evolution law of compressive strength of mudstone under different water content. With the increase in water content, the compressive strength decreased from 20.2 to 3.3 MPa, and the compressive strength decreased by 84%. In Figure 4B, the law of tensile strength enhancement of mudstone under different water content. With the increase in water content, the tensile strength decreased from 5.7 to 1.02 MPa, and the compressive strength decreased by 82.1%. According to the data fitting in Figure 4, the elastic modulus, shear modulus, and tensile strength of rock under different water contents are obtained. The functional relationship is as follows:

$$\begin{cases} y_1 = 3.7251e^{-1.0w} + 0.82509 \\ y_2 = 15.7090e^{-1.045w} + 9.0847 \\ y_3 = -3.69386e^{-0.23106w} + 10.3261 \end{cases} \quad (2)$$

where y_1, y_2, and y_3 are shear modulus, bulk modulus, and tensile strength, Mpa; w is the moisture content, %.

TABLE 1 Model meso-initial parameters.

Meso parameters	Symbol	Numerical value
Minimum particle radius/m	R_{min}	0.5e-3
Maximum to minimum particle radius ratio	R_{max}/R_{min}	1.5
Particle density/kg/m^3	ρ	2,500
Porosity/%	n	0.1
Damping coefficient	ζ	0.7
Particle normal to tangential contact stiffness ratio	K_n/k_s	2.5
Particle Elastic Modulus/GPa	$\bar{E_c}$	3
Parallel Bond Radius Coefficient	$\bar{\lambda}$	1.0
Friction coefficient	μ	0.9

TABLE 2 Physical and mechanical parameters of coal and rock.

Name	Density	Bulk modulus	Shear modulus	Cohesion	Internal friction angle/°	Tensile strength
	g/cm^3	/GPa	/GPa	/MPa		/MPa
Basic roof	2,873	1.84	0.80	2.3	28	2.0
Immediate roof	2,487	y_1	y_2	1.9	30	y_3
3#coal	1,400	1.66	0.85	2.1	32	1.28
Immediate floor	2,483	1.84	0.80	2.3	28	2.0
Basic floor	2,460	1.79	0.97	1.9	30	1.6

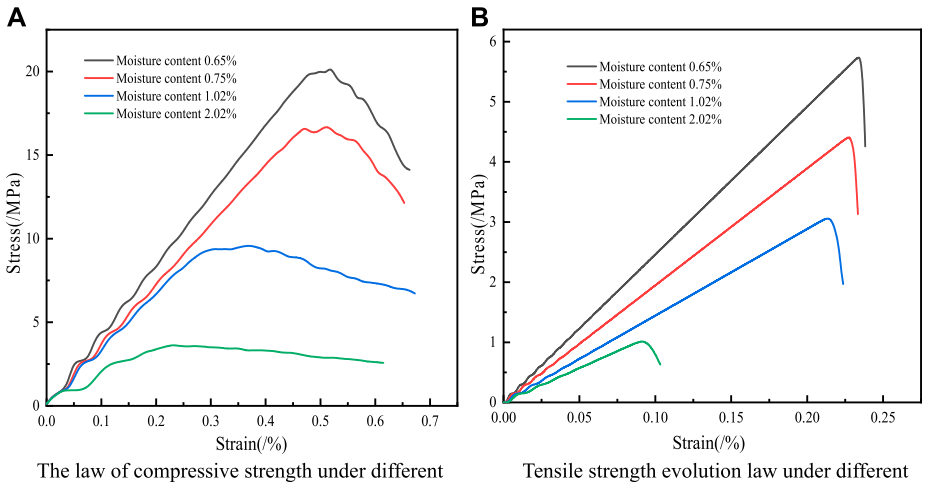

FIGURE 4
Evolution law of mudstone mechanical properties under different water content. **(A)** The law of compressive strength under different moisture content. **(B)** Tensile strength evolution law under different moisture content.

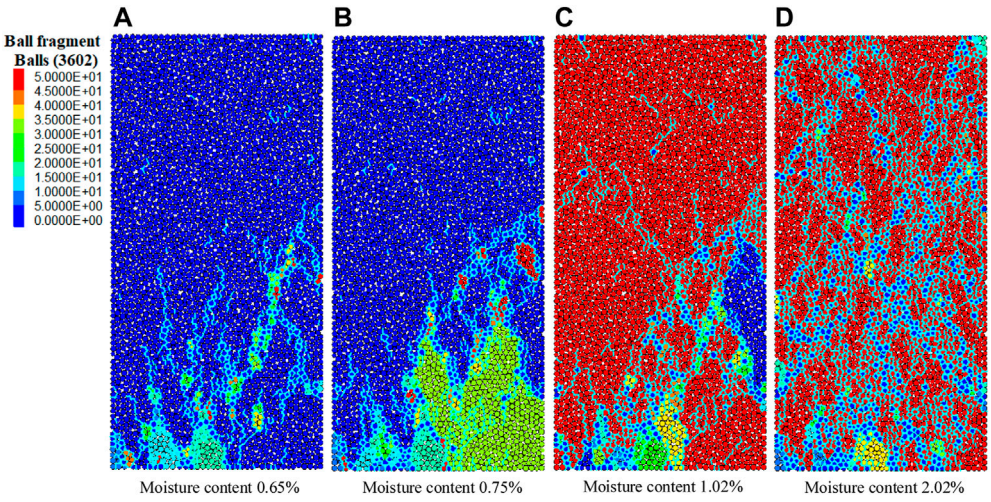

FIGURE 5
Evolution law of rock compression cracks. **(A)** Moisture content 0.65% **(B)** Moisture content 0.75% **(C)** Moisture content 1.02% **(D)** Moisture content 2.02%

Evolution law of mudstone fissures under different water contents

Figure 5 shows the crack evolution law of rock under compression under different water contents. In Figure 5A, when the water content of mudstone is 0.65%, the bottom of the sample cracks, and the cracks are mainly concentrated in the lower part of the sample. In Figure 5B, when the moisture content increases to 0.75%, the cracks extend from bottom to top, the number of cracks increases, and the lower-left sample breaks. In Figure 5C, when the moisture content increased to 1.02%, the entire sample was damaged, and the crack penetrated the middle and upper part of the sample. In Figure 5D, when the moisture content is 2.02%, the entire sample is broken, and the crack penetrates the entire sample. In summary, with the increase of water content, the number of crack penetrations increases, providing channels for the movement of water molecules, resulting in crack expansion and rock softening.

Figure 6 shows the crack evolution law of rock under tension under different water contents. In Figure 6A, when the moisture

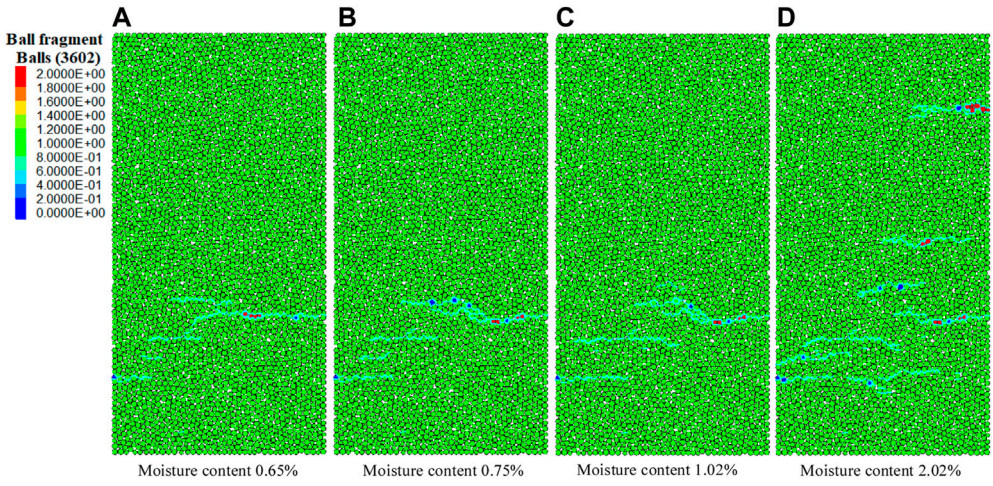

FIGURE 6
Evolution law of tensile cracks in rock. Please add a legend **(A)** Moisture content 0.65% **(B)** Moisture content 0.75% **(C)** Moisture content 1.02% **(D)** Moisture content 2.02%

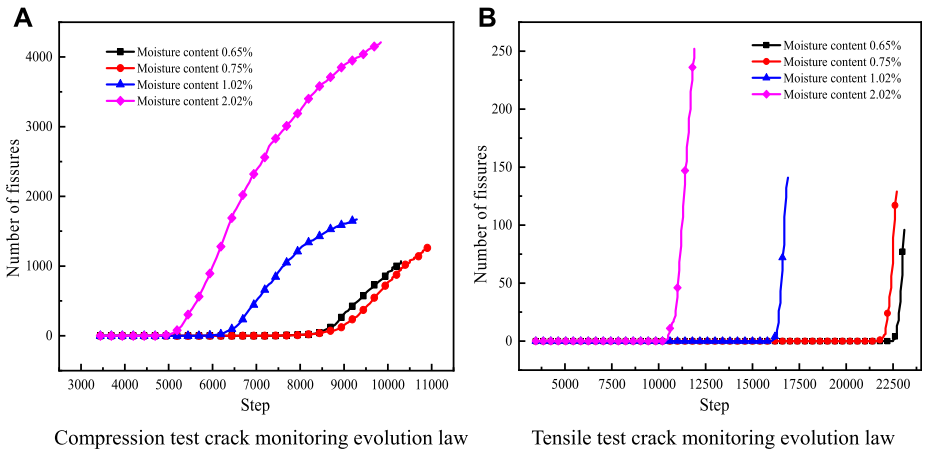

FIGURE 7
Evolution law of crack monitoring. **(A)** Compression test crack monitoring evolution law. **(B)** Tensile test crack monitoring evolution law.

content is 0.65%, the tensile failure of the sample occurs in the lower part. In Figure 6B, when the moisture content is 0.75%, tensile failure occurs in the lower part of the sample, and the crack expansion length increases. In Figure 6C, when the moisture content is 1.02%, tensile failure occurs in the lower part of the sample, mainly showing three macroscopic cracks. In Figure 6D, when the moisture content is 2.02%, the overall tensile failure of the sample occurs. In summary, with the increase of water content, the internal cementation of the rock decreases, the bonding force between the rock molecules decreases, and the tensile strength of the surrounding rock deteriorate.

Figure 7 shows the evolution law of crack monitoring of mudstone under uniaxial compression and tensile tests. In Figure 7A, when the mudstone with a moisture content of 2.02% is subjected to a uniaxial compression test under the same conditions, cracks are generated first and the number of cracks is the largest. Figure 7B shows the evolution law of crack monitoring in the mudstone tensile test under different water contents. The time of crack appearance from early to late is moisture content 2.02%> moisture content 1.02%> moisture content 0.75%> moisture content 0.65%. The maximum number of cracks in the sample with a moisture content of

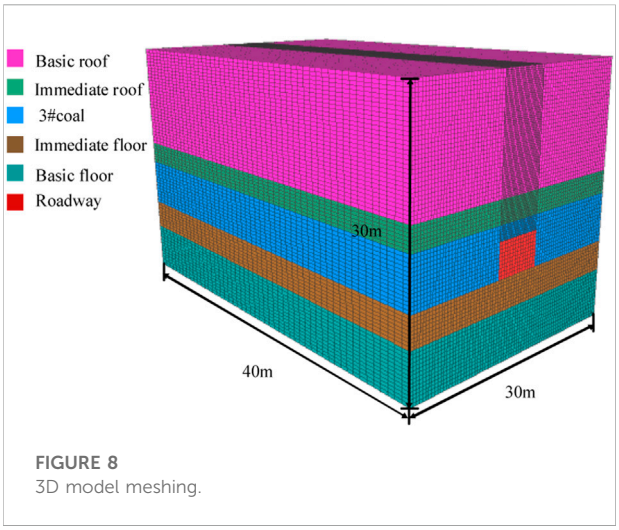

FIGURE 8
3D model meshing.

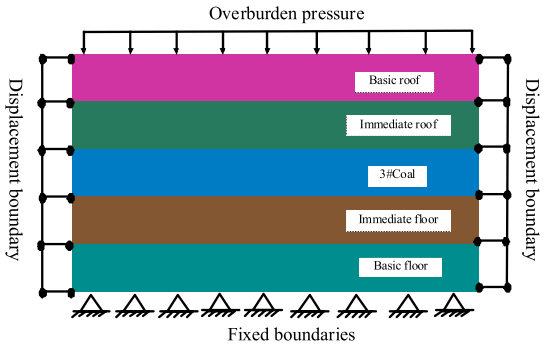

FIGURE 9
Static calculation model.

2.02% is 252, and the minimum number of cracks in the sample with a moisture content of 0.65% is 96. To sum up, as the water content increases, the earlier the mudstone is damaged, the more cracks and the greater the softening degree.

Failure and evolution law of roadway surrounding rock under different moisture content

According to the geological situation of the Zhangcun coal mine, transport roadway 2,606 was selected as the research object. The FLAC^{3D} software was used to establish the computational model, and the effect of moisture content on the unstable deformation of the roadway was analyzed by using the coupling of large deformation and hydrostatic modules. It should be noted that pores and joint fissures of various morphologies in the natural coal rock structure were not considered (Wang et al., 2021). The model was assumed to be isotropic and the Moore Coulomb criterion was used in the simulation (Jia et al., 2021). The physical and mechanical parameters of the surrounding rock were fitted into the moisture content relationship curve as exponential functions of y_1~y_3. The model was assigned by compiling the function in the FISH language. Table 2 shows the specific parameters of the model. The size of the model is 30 m × 40 m × 30 m (length × width × height), as shown in Figure 8. The roadway is excavated along the No.3 coal floor, with a rectangular section and a size of 5.8m × 4 m (width × height). Figure 9 shows the overall model. In the static calculation, the left and right boundaries of the model are constrained by horizontal hinges, the bottom boundary is fixed and constrained, and the upper boundary is free and bears the uniform load acting on the boundary by the overburden.

Evolution law of displacement field of roadway surrounding rock

Figure 10 illustrates the effect of different moisture contents on the displacement change of roof, floor and two sides of the roadway. Monitoring points were arranged at the roof and floor of the roadway and in the middle of the two sides to monitor the displacement of the surrounding rock. Figure 10A shows the failure deformation of surrounding rock and roof subsidence caused by initial rock stress field failure at the initial stage of roadway excavation. With the continuous increase of the moisture content, the vertical displacement and subsidence of the roof also increase. Before the time step of 18,000 step, the roof subsidence changes drastically, and the subsidence amount tends to be stable from 18,000 step to 22,000 step, reaching a new equilibrium state. The increase in moisture content leads to the softening of the top coal, and the top coal is more likely to be broken and deformed. Figure 10B shows that the bottom heave phenomenon occurs in the floor, and the moisture content has little effect on the bottom heave of the roadway floor. Figure 10C shows the relationship between the left side of the roadway and the moisture content. As the moisture content increases, the horizontal displacement of the left side increases. When the moisture content increases from 0.67 to 2.02%, the maximum displacement of the left side deformation increases from 19.47 to 53.75 mm, increasing by 67.49%. Figure 10D shows the relationship between the right side of the roadway and the moisture content. With the excavation of the roadway, the horizontal displacement of the right side occurs, which increases rapidly at first and then gradually changes steadily. With the increase of moisture content, the maximum horizontal displacement of the right side also increases, and the maximum value reaches 53.45 mm. The above analysis shows that water drenching has a serious impact on the displacement of the roof and has the least impact on the floor. According to the analysis of on-site drilling exploration data, it can be found that No. VII on the

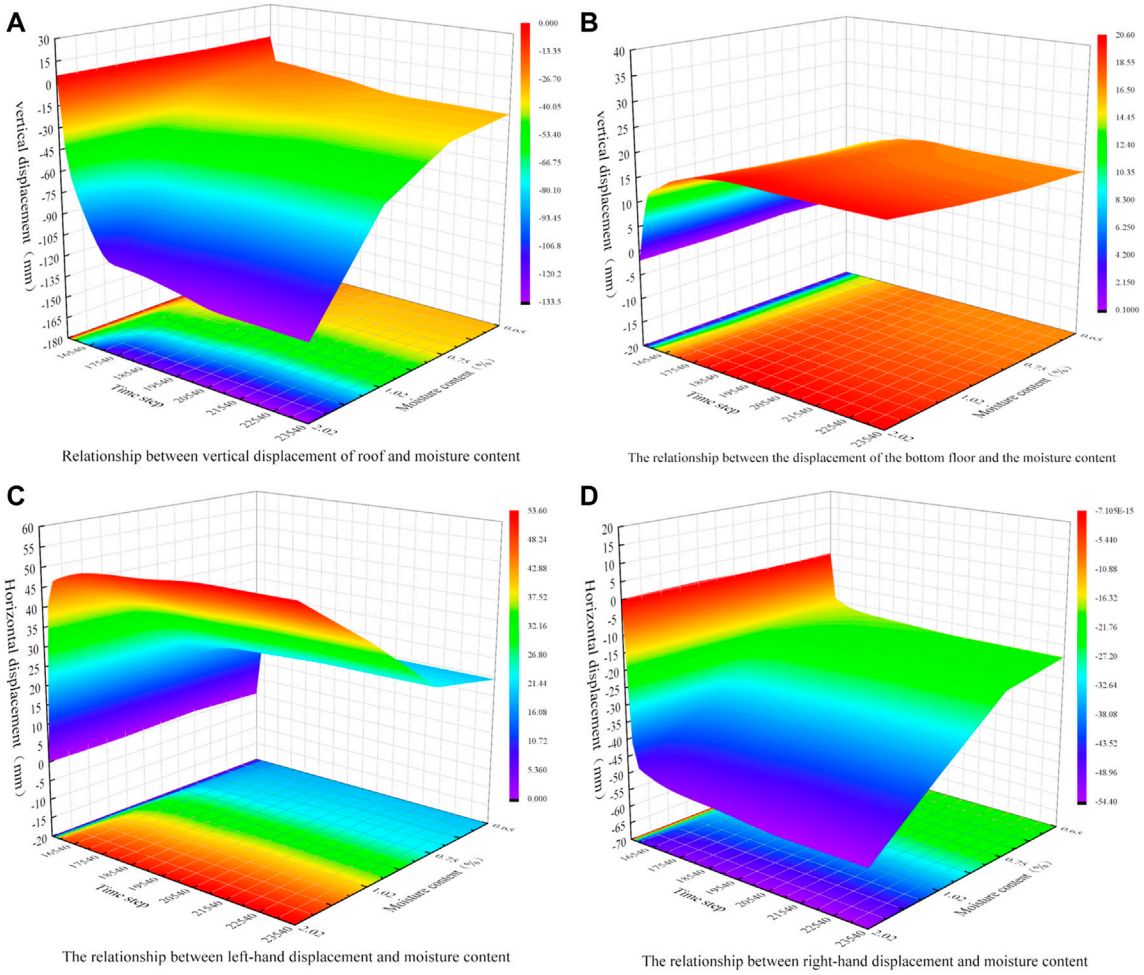

FIGURE 10
Relationship between deformation of surrounding rock and water content of roadway. **(A)** The relationship between vertical displacement of roof and moisture content **(B)** The relationship between vertical displacement of floor and moisture content **(C)** The relationship between horizontal displacement of left side and moisture content **(D)** The relationship between horizontal displacement of right side and moisture content

roof of the No. 3 coal seam is an aquifer that has a great influence on the roof, which is in line with the actual situation on site.

In Figure 11, exponential fitting is performed between the displacement of the roof, floor and two sides and the water content, and four exponential equations are obtained as y_1-y_4. The exponential relationship between roof displacement and water content is represented by equation y_1, and R^2=0.99 has a significant fitting effect. The exponential relationship between the displacement of the right side and the water content is represented by the equation y_2, and the fitting effect of R^2=0.98 is significant. The exponential relationship between the displacement of the left side and the water content is represented by the equation y_3, and the fitting effect of R^2=0.98 is significant. The exponential relationship between the displacement of the bottom plate and the water content is represented by the equation y_4, and the fitting effect of R^2=0.99 is significant. To sum up, the relationship between surrounding rock deformation and water content can be significantly described by exponential equation, which provides a reference for water drenching roadway support.

Evolution law of plastic zone of roadway surrounding rock

Figure 12 shows the failure evolution law of the plastic zone of the surrounding rock of the roadway under different moisture contents. The grid in the model is divided into 0.2 m. According to Figure 12A, the plastic zone failure range is 1.8 m away from the roof, and tensile failure occurs

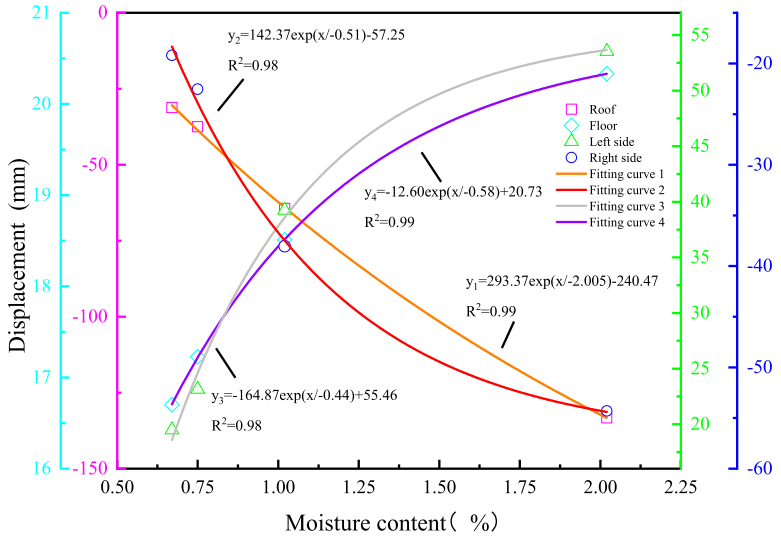

FIGURE 11
Prediction of surrounding rock displacement under different moisture contents.

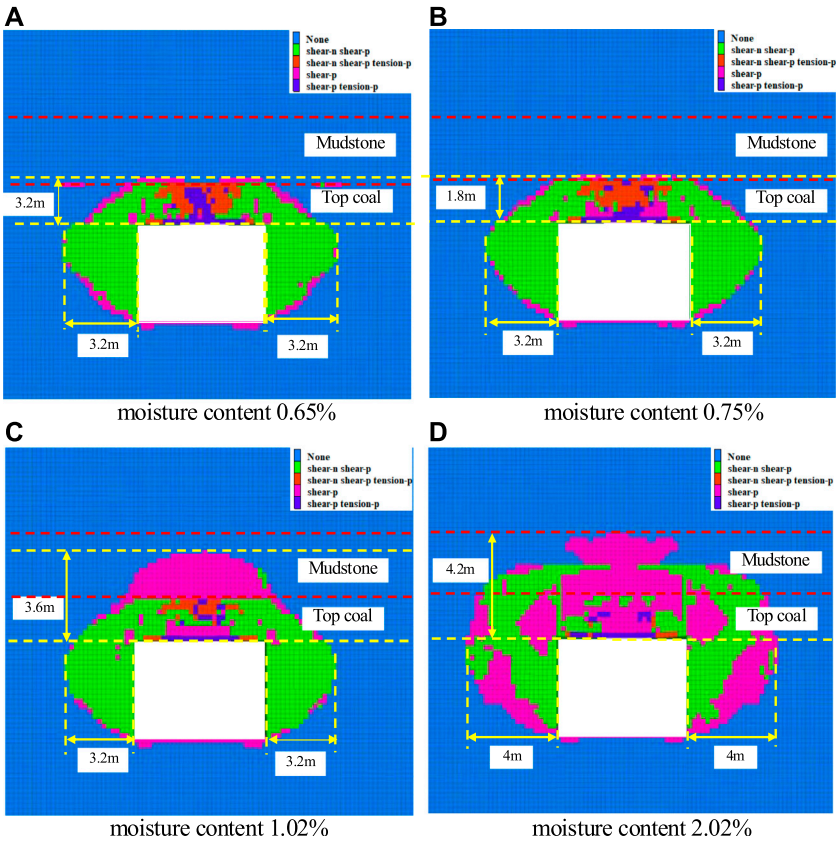

FIGURE 12
Evolution law of surrounding rock plastic zone under different water content. **(A)** Moisture content 0.65% **(B)** Moisture content 0.75% **(C)** Moisture content 1.02% **(D)** Moisture content 2.02%.

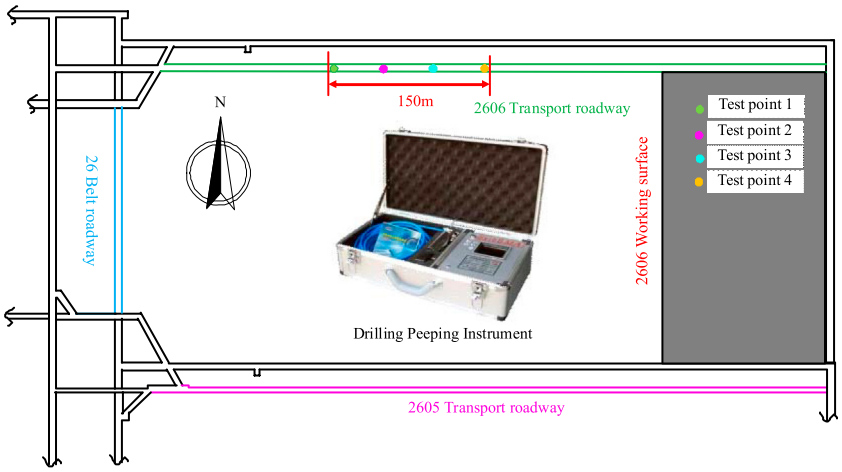

FIGURE 13
Location of roadway and test points for experimental tests.

at the coal-rock interface. As shown in Figures 12A,B, there are the same plastic zone failure ranges, but a large amount of tensile failure occurs at the coal-rock interface, and the top coal failure is more serious. The roofs in Figure 12A and Figure 12B will appear integral separation phenomenon. In this case, the supporting density of anchor cables should be increased, and the pre-tightening force should be increased. As shown in Figure 12C, the failure range of the plastic zone extends to 3.6 m from the roof. At this time, all the top coal is destroyed, and a large amount of mudstone is destroyed. The pores in the coal continuously absorb water, the strength of mechanical characteristics decreases, the lithological strength of mudstone is relatively soft, leading to the serious damage. It can be seen from Figure 12D that the failure range of the plastic zone extends to 4.2 m from the roof. The mudstone above the roof is completely destroyed, and a large number of shear failures occur. The bending failure occurs in the roof of Figure 12C and Figure 12D. At this point, the bolt should be passed through multiple separation positions and anchored deep into the stable rock formation. It can be seen from Figures 12A–D that the water drenching has a serious impact on the damage of the roadway roof, and there is no obvious change in the plastic zone of the two sides and the floor. At the coal-rock interface, tensile failure occurs, and coal-rock separation occurs. During the excavation process, due to the continuous infiltration of groundwater into the roof, the pores of the coal and rock mass themselves continuously absorb water, and the moisture content increases. As a result, the strength of the roof is reduced, and the weakening of the supporting capacity of the anchor rod and anchor cable is caused. The failure depth above the roof of the plastic zone increases, and the water drenching roadway has the most serious impact on the roof.

Field experiment of water–drenching roadway

In Zhangcun coal mine, the experimental test is located at 150 m of roadway, and 4 test points are arranged with the interval of 50 m. The borehole peeping instrument was used to conduct on-site experiments, as shown in the Figure 13.

Drilling peep in 2,606 roadway roof

The roof drilling detector was used for borehole peeping on the roof of four test points. The hole depth of each borehole is 9.6 m and the hole diameter is 30 mm, which is completely perpendicular to the roof. Figure 14 shows the drilling image of the roof fracture development. Figures 14A,B is the drilling peep results of test points1-4. As shown in Figure 14A, when the drilling depth is 0.8m and 1.1–1.3 m, there are slight local fissures, and the lithology is sandy mudstone with soft hardness, and the color of the returned water is grayish black. According to the above plastic zone distribution, the roof plastic zone failure is less than 1.8 m, and the moisture content is less than 0.65%. In Figure 14B, there is a slight fissure at the drilling depth of 2.4 m, and the lithology is sandstone with high hardness, and the color of the returned water is grayish-white. According to the above distribution law of plastic zone, the failure range of roof plastic zone is 1.8–3.6 m, and the moisture content is 0.65–1.02%. As shown in Figure 14C, when the drilling depth is 3–4.0 m, the lithology is mudstone, hard-soft rock. The hole wall is rough, pitted, and uneven, and the color of the returned water is black. According to the above distribution of plastic zone, the moisture content is less than 2.02%. In Figure 14D, at the

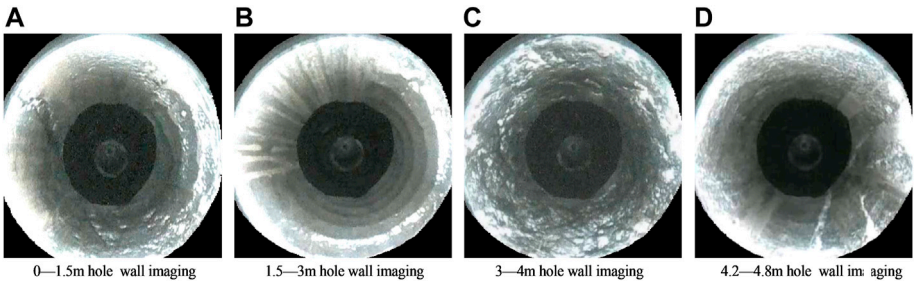

FIGURE 14
Fracture development in the roof detected by drilling image. **(A)** 0–1.5 m hole wall imaging **(B)** 1.5–3 m hole wall imaging **(C)** 3–4 m hole wall imaging **(D)** 4.2–4.8 m hole wall imaging.

drilling depth of 4.2–4.8 m, there is local breakage with slight fissures, the lithology is muddy sandstone with hard hardness, and the color of the returned water is gray and black. According to the above distribution law of plastic zone, the moisture content is greater than 2.02%.

Conclusion

1) There is a negative exponential relationship between water content and compressive strength, elastic modulus and tensile strength of coal. The instability failure law of the surrounding rocks of the roadway with different moisture contents is obtained. The influence of moisture content on the surrounding rock can be ordered as roof > two sides > floor.
2) The exponential equations of the moisture content rate and the displacement stability value of roof, floor and two sides of the roadway are obtained.
3) The water content ranges of four test points were obtained by comparing the borehole peeping results with the failure range of plastic zone. Provide theoretical guidance for roadway surrounding rock zoning support.

Data availability statement

The original contributions presented in the study are included in the article/Supplementary Material, further inquiries can be directed to the corresponding author.

Author contributions

All authors contributed to the study conception and design. Data collection and analysis were performed by CJ, SL, CF, ML, ZY, LY, and ZP. All authors read and approved the final manuscript.

Funding

This research was financially supported by the National Natural Science Foundation of China (Grant Nos. 52074146 and 51874159).

Acknowledgments

The authors would like to thank all editors and reviewers for their comments and suggestions.

Conflict of interest

ML was employed by the Company Shanxi Lu'an Chemical (Group) Co., Ltd.

The remaining authors declare that the research was conducted in the absence of any commercial or financial relationships that could be construed as a potential conflict of interest.

Publisher's note

References

Bai, Q. S., and Tu, S. H. (2016). Failure analysis of a large span longwall drift under water-rich roofs and its control techniques. *Eng. Fail. Anal.* 67, 15–32. doi:10.1016/j.engfailanal.2016.05.028

Castro-Filgueira, U., Alejano, L. R., Arzúa, J., and Ivars, D. M. (2017). Sensitivity analysis of the micro-parameters used in a PFC analysis towards the mechanical properties of rocks. *Procedia Eng.* 191, 488–495. doi:10.1016/j.proeng.2017.05.208

Chen, D. H., Chen, H. E., Zhang, W., Lou, J. Q., and Shan, B. (2021). An analytical solution of equivalent elastic modulus considering confining stress and its variables sensitivity analysis for fractured rock masses. *J. Rock Mech. Geotechnical Eng.* 14, 825–836. doi:10.1016/j.jrmge.2021.08.007

Chen, S., Wu, A., Wang, Y., Chen, X., Yan, R., and Ma, H. (2018). Study on repair control technology of soft surrounding rock roadway and its application. *Eng. Fail. Anal.* 92, 443–455. doi:10.1016/j.engfailanal.2018.06.006

Chen, Y., Li, Q., Pu, H., Liang, C., Deyu, Q., Xuyang, S., et al. (2020). Modeling and simulation of deformation mechanism of soft rock roadway considering the mine water[J]. *Geofluids* 2020. doi:10.1155/2020/8812470

Dou, Z., Tang, S. X., Zhang, X. Y., Liu, R. C., Zhuang, C., Wang, J. G., et al. (2021). Influence of shear displacement on fluid flow and solute transport in a 3D rough fracture. *Lithosphere* 2021, 1569736. doi:10.2113/2021/1569736

Fan, C., Li, S., Elsworth, D., Han, J., and Yang, Z. (2020). Experimental investigation on dynamic strength and energy dissipation characteristics of gas outburst-prone coal. *Energy Sci. Eng.* 8 (4), 1015–1028. doi:10.1002/ese3.565

Fan, C., Wen, H., Li, S., Bai, G., and Zhou, L. (2022). Coal seam gas extraction by integrated drillings and punchings from floor roadway considering hydraulic-mechanical coupling effect[J]. *Geofluids* 2022, 5198227. doi:10.1155/2022/5198227

Fan, C., Wen, H., Sun, H., Zhou, L., Zhang, X., Zhu, C., et al. (2022). Experimental investigation on the effect of loading and unloading on coal permeability with different sediment beddings[J]. *Lithosphere* 2022, 9949201. doi:10.2113/2022/9949201

Fan, C., Yang, L., Wang, G., Huang, Q., Fu, X., and Wen, H. (2021). Investigation on coal skeleton deformation in CO2 injection enhanced CH4 drainage from underground coal seam. *Front. Earth Sci. (Lausanne).* 9, 766011. doi:10.3389/feart.2021.766011

Gao, M. Z., Xie, J., Gao, Y. N., Wang, W. Y., Li, C., Yang, B. G., et al. (2021). Mechanical behavior of coal under different mining rates: A case study from laboratory experiments to field testing. *Int. J. Min. Sci. Technol.* 31 (2021), 825–841. doi:10.1016/j.ijmst.2021.06.007

He, M. C. (2014). Progress and challenges of soft rock engineering in depth[J]. *J. China Coal Soc.* 39 (8), 1409–1417. doi:10.13225/j.cnki.jccs.2014.9044

He, Q. (2021). *Instability mechanism of surrounding rock in weakly cemented roadway under force-water coupling [D]*. Hebei Engineering University. doi:10.27104/d.cnki.ghbjy.2021.000571

Jia, C., Li, S., Fan, C., and Tang, J. (2021). Numerical simulation of mechanical characteristics of roadway surrounding rock under dynamic and static loading. *Shock Vib.* 2021–16. doi:10.1155/2021/1869583

Jing, H., Yin, Q., Yang, S., and Chen, W. (2021). Micro-mesoscopic creep damage evolution and failure mechanism of sandy mudstone. *Int. J. Geomech.* 21 (3), 04021010. doi:10.1061/(asce)gm.1943-5622.0001940

Li, G., Jiang, Z., Lv, C., Huang, C., Gui, C., and Li, M. (2015). Instability mechanism and control technology of soft rock roadway affected by mining and high confined water. *Int. J. Min. Sci. Technol.* 25 (04), 573–580. doi:10.1016/j.ijmst.2015.05.009

Li, S., Liu, R., Zhang, Q., and Zhang, X. (2016). Protection against water or mud inrush in tunnels by grouting: A review. *J. Rock Mech. Geotechnical Eng.* 8 (5), 753–766. doi:10.1016/j.jrmge.2016.05.002

Liu, B., Yang, H., and Karekal, S. (2020). Effect of water content on argillization of mudstone during the tunnelling process. *Rock Mech. Rock Eng.* 53 (2), 799–813. doi:10.1007/s00603-019-01947-w

Liu, C. D., Cheng, Y., Jiao, Y. Y., Zhang, G. H., Zhang, W. S., Ou, G. Z., et al. (2021). Experimental study on the effect of water on mechanical properties of swelling mudstone. *Eng. Geol.* 295, 106448. doi:10.1016/j.enggeo.2021.106448

Ma, C., Xu, J., Tan, G., Xie, W., and Lv, Z. (2021). Research on supporting method for high stressed soft rock roadway in gentle dipping strata of red shale. *Minerals* 11 (4), 423. doi:10.3390/min11040423

Su, Y. Q., Gong, F. Q., Luo, S., and Liu, Z. X. (2021). Experimental study on energy storage and dissipation characteristics of granite under two-dimensional compression with constant confining pressure. *J. Cent. South Univ.* 28 (3), 848–865. doi:10.1007/s11771-021-4649-2

Tao, Z., Cao, J., Yang, L., Guo, A., Huang, R., Yang, X., et al. (2020). Study on deformation mechanism and support measures of soft surrounding rock in muzhailing deep tunnel. *Adv. Civ. Eng.* 2020, 1–14. doi:10.1155/2020/9367916

Wang, X., Li, Y., Zhao, C., Wang, Y., and Huang, S. (2021). Study on deformation failure mechanism and control technology of surrounding rock in soft rock roadway. *Geotech. Geol. Eng. (Dordr).* 39 (8), 5931–5942. doi:10.1007/s10706-021-01977-8

Wang, Y., Yang, H. N., Han, J. Q., and Zhu, C. (2022). Effect of rock bridge length on fracture and damage modelling in granite containing hole and fissures under cyclic uniaxial increasing-amplitude decreasing-frequency (CUIADF) loads. *Int. J. Fatigue* 158, 106741. doi:10.1016/j.ijfatigue.2022.106741

Wen, W., Zhang, S., Xiao, T., Hao, Y., Li, D., and Li, H. (2021). Factors that affect the stability of roads around rocks. *Geomatics, Nat. Hazards Risk* 12 (1), 829–851. doi:10.1080/19475705.2021.1895327

Xie, H., Ju, Y., Gao, M., and Gao, F. (2018). Theories and technologies for *in-situ* fluidized mining of deep underground coal resources[J]. *J. China Coal Soc.* 43 (5), 1210–1219. doi:10.13225/j.cnki.jccs.2018.0519-cn

Yang, R., Li, Y., Guo, D., Yao, L., Yang, T., and Li, T. (2017). Failure mechanism and control technology of water-immersed roadway in high-stress and soft rock in a deep mine. *Int. J. Min. Sci. Technol.* 27 (2), 245–252. doi:10.1016/j.ijmst.2017.01.010

Yang, S. Q., Chen, M., Jing, H. W., Chen, K. F., and Meng, B. (2017). A case study on large deformation failure mechanism of deep soft rock roadway in Xin'An coal mine, China. *Eng. Geol.* 217, 89–101. doi:10.1016/j.enggeo.2016.12.012

Yang, S. Q., Tian, W. L., Jing, H. W., Huang, Y. H., Yang, X. X., and Meng, B. (2019). Deformation and damage failure behavior of mudstone specimens under single-stage and multi-stage triaxial compression. *Rock Mech. Rock Eng.* 52 (3), 673–689. doi:10.1007/s00603-018-1622-y

Yu, W., Li, K., Liu, Z., An, B., Wang, P., and Wu, H. (2021). Mechanical characteristics and deformation control of surrounding rock in weakly cemented siltstone. *Environ. Earth Sci.* 80 (9), 1–15. doi:10.1007/s12665-021-09626-2

Zhai, W., He, F., Xu, X., Lv, K., Li, L., and Song, J. (2022). Floor heave mechanism in water-rich soft rock roadways and a DS-IBA control approach. *Geomat. Nat. Hazards Risk* 13 (1), 2107–2123. doi:10.1080/19475705.2022.2107439

Zhang, Q. B., He, L., and Zhu, W. S. (2016). Displacement measurement techniques and numerical verification in 3D geomechanical model tests of an underground cavern group. *Tunn. Undergr. Space Technol.* 56, 54–64. doi:10.1016/j.tust.2016.01.029

Zhao, B., Wen, G., Nian, J., Ma, Q., Fan, C., Lv, X., et al. (2022). Numerical simulation study on the multi-physical field response to underground coal and gas outburst under high geo-stress conditions. *Minerals* 12, 151. doi:10.3390/min12020151

Zhao, K., Yang, D., Zeng, P., Huang, Z., Wu, W., Li, B., et al. (2021). Effect of water content on the failure pattern and acoustic emission characteristics of red sandstone. *Int. J. Rock Mech. Min. Sci.* 142, 104709. doi:10.1016/j.ijrmms.2021.104709

Zheng, L., Zuo, Y., Hu, Y., and Wu, W. (2021). Deformation mechanism and support technology of deep and high-stress soft rock roadway. *Adv. Civ. Eng.* 2021–14. doi:10.1155/2021/6634299

Zhu, C., Karakus, M., He, M. C., Meng, Q. X., Shang, J. L., Wang, Y., et al. (2022). Volumetric deformation and damage evolution of Tibet interbedded skarn under multistage constant-amplitude-cyclic loading. *Int. J. Rock Mech. Min. Sci.* 152, 105066. doi:10.1016/j.ijrmms.2022.105066

Zhu, Z., Wu, Y., and Han, J. (2022). A prediction method of coal burst based on analytic hierarchy process and fuzzy comprehensive evaluation. *Front. Earth Sci.* 9, 834958. doi:10.3389/feart.2021.834958